Hippocampal Context Switches

Joel Shor

Advisor: Professor David Tank

Professor Philip Holmes

Submitted in partial fulfillment

of the requirements for the degree of

Bachelor of Arts

Department of Mathematics

Princeton University

June 2014

This thesis represents my own work in accordance with University regulations.

_____

Joel Shor

Abstract

The hippocampus is an area of the brain important to memory and spatial reasoning. Despite being heavily researched, there are still many phenomena that are poorly understood. One such phenomenon, called global remapping, occurs when spatially-dependent neurons change their firing patterns. There is ample evidence to show that a rat's hippocampus undergoes global remapping when introduced to a new environment, but recent studies have shown that remapping can occur in the same place when the rat is performing the same task. In this paper, we review the history and motivation for this problem and present an experiment that seeks to identify when a rat's hippocampus remaps. We develop a machine learning algorithm that can be used to analyze the results of the experiment to determine the moments in time when global remapping occurs.

Acknowledgements

Thanks to Dmitriy Aronov for coaching me through the research process. I am especially grateful for Dayton 'Cool Kid' Martindale, Kim 'Chi' Freid, Elan 'EPK' Kugelmass, Parinda 'The Boss' Wanitwat, and the rest of my 2D friends for their comfort and support.

Contents

Chapter 1

Introduction

Modern neuroscience experiments produce too much data to be analyzed by hand, but the underlying processes are too elusive to be easily learned by a machine. Neuroscience utilizes electrical recording devices that sample output from thousands of cells at once at a rate of tens of thousands of times per second, and it can be difficult if not impossible for a single person to look at the entire results of an experiment. However, the data may also contain noise, overlap, and recording abnormalities so that only a trained expert can make sense of the underlying patterns. Although computers are always getting faster, there is still an enumerable list of problems that the human mind is better at. Among these are many of the basic problems that neuroscientists face, such as recognizing legitimate cell output from background noise and identifying patterns in neuronal output. The difficulty in these problems mean that they cannot be overcome simply by doing things more rapidly. Instead, we need smarter way of processing data and detecting underlying patterns. This is where the field of machine learning, which studies how we can create theoretical and practice tools that automatically structure data, becomes invaluable.

This thesis seeks to apply machine learning techniques to analyze a poorly-understood neuroscience phenomenon called global remapping. Specifically, we seek to develop

an algorithm that can identify exactly when this phenomenon occurs in rats given only position data and electrical recordings from the brain. We will give neuroscience background and motivation for the problem in Chapter 2. An overview of the experimental and theoretical neuroscience tools used will be given in Chapters 3 and 4. We will then present the experimental setup that was used to collect our data in Chapter 5. Chapter 6 will serve as an introduction to the problem that we address and the machine learning tools that we use in a more general framework. Readers already familiar with machine learning terminology and the tools presented can skip this chapter. We then present our analysis and results in Chapters 7 and conclude in Chapter 9 with a discussion of how our results further our understanding of the brain.

Chapter 2

The Hippocampus

In this chapter, we present the neuroscience background necessary to understand the context of the machine learning problem that we address. We provide the reader with a historical view of the hippocampus. Beginning with the study of a famous amnesiac that linked the hippocampus to memory (Section 2.1), we proceed to describe the evidence for the hippocampus's role in memory (Section 2.2) and spatial reasoning (Section 2.3). We then present newer evidence that indicates that neither the memory nor spatial reasoning roles tell the whole story (Section 2.4). Finally, we present a relatively recently discovered hippocampal phenomenon called 'global remapping' that is the focus of this study (Section 2.5).

2.1 H.M.

Henry Molaison, more commonly referrred to as H.M., is perhaps the most famous patient in neuroscience history. Born in 1926 and suffering from medically intractable epilepsy, H.M. underwent radical and experimental surgery that involved the removal of the two hippocampi on either side of his brain (Figure 2.1). There were two primary results of his surgery. First, H.M.'s seizures decreased steadily, settling at roughly 2 per year in 2002. The second result, which was first described in a 1957 paper

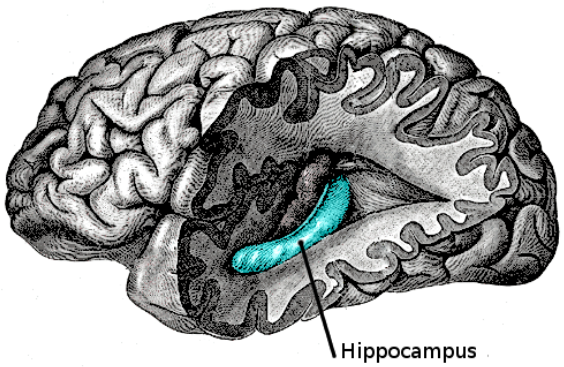

Figure 2.1: The location of the hippocampus in humans.

(Scoville and Milner), is that he suffered from severe anterograde amnesia as well as partial retrograde amnesia. In other words, H.M. retained his ability to remember things temporarily, such as recalling what was just said in order to participate in a conversation, and to learn procedures, such as tying his shoes. However, he could not make new explicit memories, such as remembering his schedule or the current president, and could not remember some events as far back as 11 years before his surgery (Corkin, 2002).

In contrast to his deficits in episodic memory and semantic memory (Section 2.2), H.M. was able to acquire new motor skills without explicitly remembering that he had learned them. One example comes from a mirror tracing task (Corkin, 2002), where H.M. was able to draw figures in a mirror at speeds comparable to control groups, yet he had no recollection of having previously performed the task. Further work (Cohen and Squire, 1980) shows that amnesiacs can retain skills such as mirror reading for more than 3 months, and can learn them at rates comparable to humans with no memory impairments (Figure 2.2)

This drastic change in certain types of memory implicates the hippocampus as being crucial to memory formation. Spurred by these findings, scientists continued to explore the link between the hippocampus and memory in animals such as rats. The results of these experiments conducted, in the 1960s and 70s, complicates the

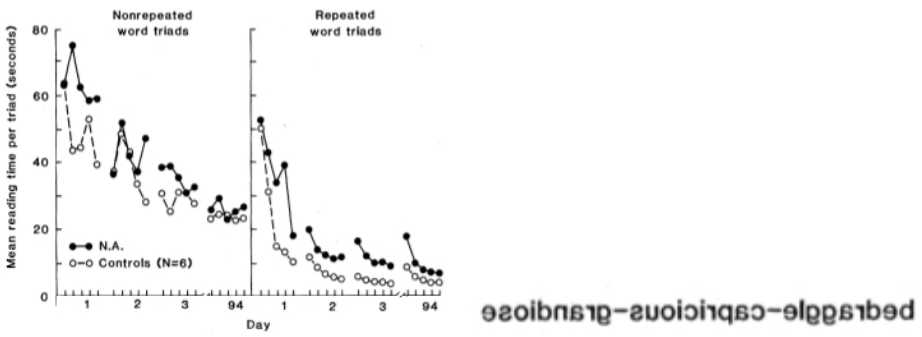

(a) (b)

Figure 2.2: Mirror task showing that amnesiacs can learn certain skills without remembering learning them. (a) Graph shows the rate at which N.A., an amnesiac patient (black), learned to read words in a mirror, and the rate at which healthy individuals (white) learned to read the same words. The left column shows the rate at which both groups read words that were new every time, and the right column shows the rate at which both groups learned the same words over a period of time. (b) An example of a stimulus presented in study. (Cohen and Squire, 1980)

picture. Rats with partially removed hippocampi can learn to press levers, run down alleys to obtain food, and avoid punishment. Peculiarly, they move around in new environments more than control rats, and continue to do so over long periods of time (Andersen et al., 2007, p. 15). In the classic T-maze paradigm, a rat runs down a track shaped like the letter 'T', making a left or a right turn at the junction (Figure 2.3). Rats with damaged hippocampi only turn one direction down these mazes, even in the absence of choice-dependent reward or punishment. They learn rewarding behavior as quickly as normal rats, but fail to adapt their behavior to a changing environment. Seemingly at odds with these results, rats with lesioned hippocampi are better at a task called 'two-way active avoidance', in which the rat moves between two boxes to avoid punishment (Andersen et al., 2007, p. 15).

2.2 Memory and the Hippocampus

The seemingly contradictory memory-related results from studies with amnesiacs, patients undergoing electroconvulsive therapy for psychiatric illness, and lesioned rats (Section 2.1) motivated scientists to propose that different types of memory relied on different regions in the brain. First, scientists distinguished between the memories

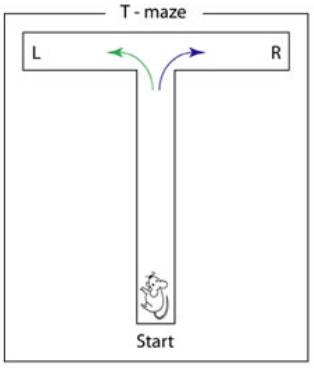

Figure 2.3: The classic T-maze paradigm, where a rat must choose between a left turn and a right turn. The rat is rewarded or punished based on its decision.

associated with a specific time and place (episodic), and the memories that represent facts about the world (semantic) (Tulving, 1972). For example, "Yesterday I adopted a puffin" is associated with a specific point in time when an action took place, whereas "All of the food that I eat is ethically sourced" is a statement of fact about the world. Although there is debate about whether this distinction has a neurological basic, it is abundantly clear that the two do not operate in isolation; semantic memory is constantly updated by episodic memory, and vice-versa.

'Declarative Memory Theory' makes a further distinction between 'declarative memory' and 'nondeclarative memory' (Figure 2.4a). Declarative memory can be consciously recalled and stated, a description which applies equally well to both episodic and semantic memory. In contrast, some examples of nondeclarative memory include learning to tie one's shoes (procedural memory), recognizing a word faster after seeing a related word just before (priming), associating two stimuli together after repeated exposure (classical conditioning), and learning that background noise is harmless and thus ignoring it (non-associative learning). In addition to making the abstract distinction between types of memory, Declarative Memory Theory also posits that the medial temporal lobe, which contains the hippocampus, is crucial to the formation and immediate storage of both types of declarative memory.

Clear evidence for the hippocampus's role in memory was presented in 1986 (Zola-

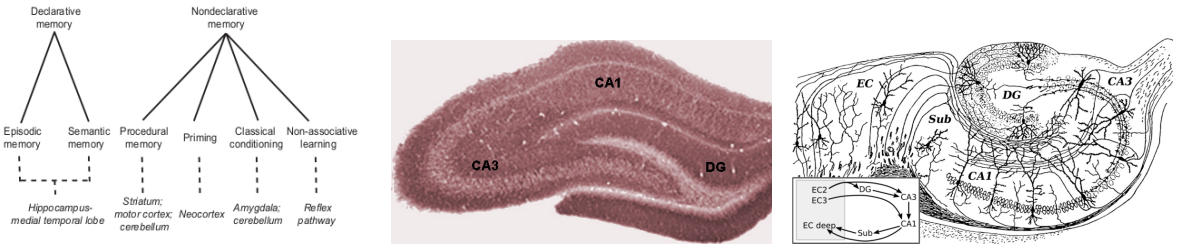

(a) (b) (c)

Figure 2.4: (a) A taxonomy of memory and their associated brain regions. (b) A labeled slice of a rat hippocampus DG stands for Dentate Gyrus. (c) A schematic diagram of the hippocampus. EC stands for entorhinal cortex, Sub stands for subiculum. (Squire, 1987)

Morgan et al.). In this paper, a patient referred to as R.B. suffered from anterograde amnesia, hardly any retrograde amnesia, and no other signs of cognitive impairment (Figure 2.5). Upon examining the patient's brain after his death, it was revealed that R.B. had damage almost exclusively confined to the CA1 region of the hippocampus. Two conclusions could be drawn from this example. First, the CA1 region in particular and the hippocampus in general plays an important role in memory storage and formation. Second, because R.B. was not as severely impaired as H.M., other structures must also be involved with memory.

2.3 The Hippocampus as a Cognitive Map

Despite the famous case of H.M. (Sec 2.1) and Declarative Memory theory linking the hippocampus to declarative memory (Sec 2.2), two categories of evidence raised doubts on how important the hippocampus was to memory. First, the results of hippocampal studies in animals were often contradictory. Removing both hippocampi in dogs allows them to learn a leg-lift response to a stimulus in only a few trials, whereas normal dogs require 40 trials or more. Rats with hippocampal lesions learn to respond to a buzzer to avoid electricity better than normal rats and those with cortical lesions. Similar results are found in other animals including monkeys and cats (Douglas, 1967). Second, damage to the hippocampus is rarely isolated, and some

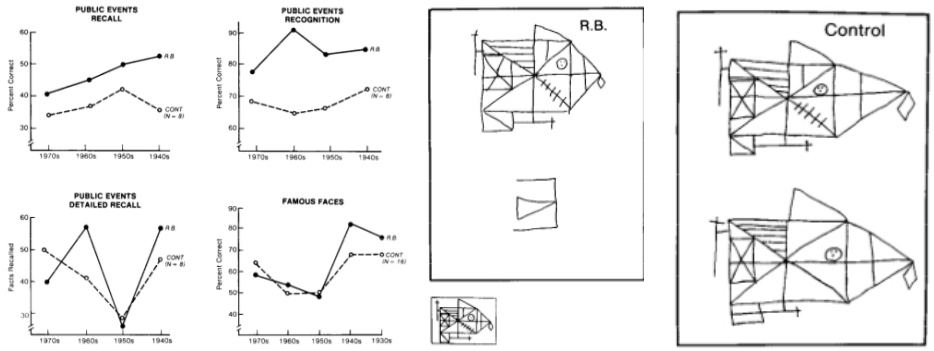

Figure 2.5: An experiment demonstrating that the CA1 specifically is crucial to memory formation. (a) Cognitive tasks showing that patient R.B. did not suffer from retrograde amnesia. In fact, he performed better than control groups (white) on most tasks. (b)(c) Two trials of a Rey-Osterreith complex figure test. Subjects were first asked to copy the small figure, then were asked to copy the figure from memory 10-20 minutes later without forewarning. R.B. ((b)) did comparable to control groups ((c)) when copying the diagram in front of him, but did poorly when asked to recall the figure.

researchers proposed that either damage to other brain areas or simultaneous damage to multiple regions were actually causing the memory deficits (Mishkin, 1978; Horel, 1978).

At the same time that scientists were developing a theory for the hippocampus's role in memory, an increasing amount of evidence suggested that the hippocampus operates as a cognitive map (Tolman, 1948; O'Keefe and Nadel, 1978). This theory posits that the main function of the hippocampus is to provide a mental map of what events happen and where they occur. The map is important to the storage, recall, and reasoning about the events and their locations (Figure 2.6). The discovery of hippocampal cells that respond to very select spatial information provides a neural mechanism to support the abstract theory of a cognitive map. This evidence was especially convincing at the time, since the theory of the hippocampus as a cognitive map predicted that such a mechanism must exist.

2.3.1 Place Cells

In 1971, O'Keefe and Dostrovsky discovered rat CA1 cells that fire when the rat is in a particular spatial region. These cells are named 'place cells', and the regions

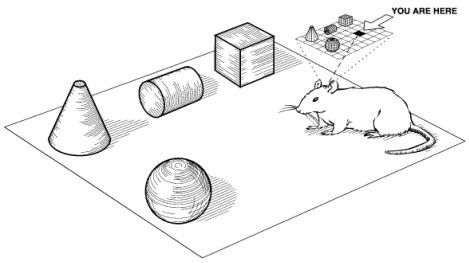

Figure 2.6: A pictorial representation of a cognitive map in a rat. (Eichenbaum et al., 1999)

in which they fire are called 'place fields' (Figure 2.7). Place cells and place fields have numerous properties that make them both easy to work with and interesting to study. Place cells close to each other in the hippocampus do not necessarily have place fields that are close to each other in the environment. Furthermore, a single place cell can have a place field in different environments, but there is no apparent relationship between the place field location in one environment when compared to the location in the other (O'Keefe and Conway, 1978). In addition, although place fields vary widely in size and shape, some location patterns have been identified: certain types of environments tend to have place fields along walls or borders, while other environments seem to have place fields randomly distributed (Andersen et al., 2007, p. 492-494). This, along with other evidence, indicates that the hippocampus plays a crucial role in spatial navigation. The place cells of the hippocampus contain so much spatial information, in fact, that a rat's location can be predicted solely on the basis of neural recordings (Wilson and McNaughton, 1993), (Figure 2.7)

2.3.2 Head Direction Cells

'Head-direction cells' (Ranck, 1984; Taube et al., 1990) are another type of spatially selective cell that are found in regions of the brain outside of the hippocampus and often have strong connections to the hippocampus proper (ex. the entorhinal cortex) (Francesca Sargolini, 2006). As their name suggests, head-direction cells fire when the rat looks in a particular direction in the horizontal plane regardless of pitch, roll,

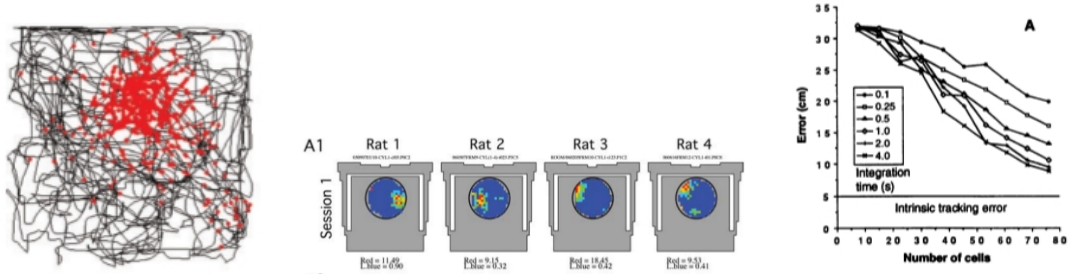

(a) (b) (c)

Figure 2.7: (a) Firing locations of a place cell superimposed over the path of a rat. (b) A heat map of place cell firing rates in various points around an environment. (c) Error reconstructing rat's path based solely on place cell activity. Plots show the error as a function of the number of cells used to predict location and the intervals of time used to estimate firing rates. (Moser et al., 2008; Fenton et al., 2008; Wilson and McNaughton, 1993)

body position, or behavior (Figure 2.8). Just like place cells, the location of the cell in the brain does not seem to correlate with the direction that the cell responds to.

2.3.3 Grid Cells

Grid cells of the medial entorhinal cortex (MEC) fire in an animal when they are located on the vertex of a hexagonal lattice tiling physical space, and they strongly innervate hippocampal place cells. A grid cell's firing pattern is determined by three parameters: grid spacing indicates the distance between vertices, angle represents the rotation of the grid, and phase represents offset in the x and y directions.

2.4 The Hippocampus and Context

2.4.1 Spatial But Not A Map

Despite the vast amount of evidence that the hippocampus encodes spatial information, is is less well-supported that the spatial information is integrated into a cognitive map. These concerns can be roughly categorized into two groups. Concerns of one type question how effective a cognitive map could be if it is based on units such as place cells. Concerns of a second type ask whether evidence actually supports the

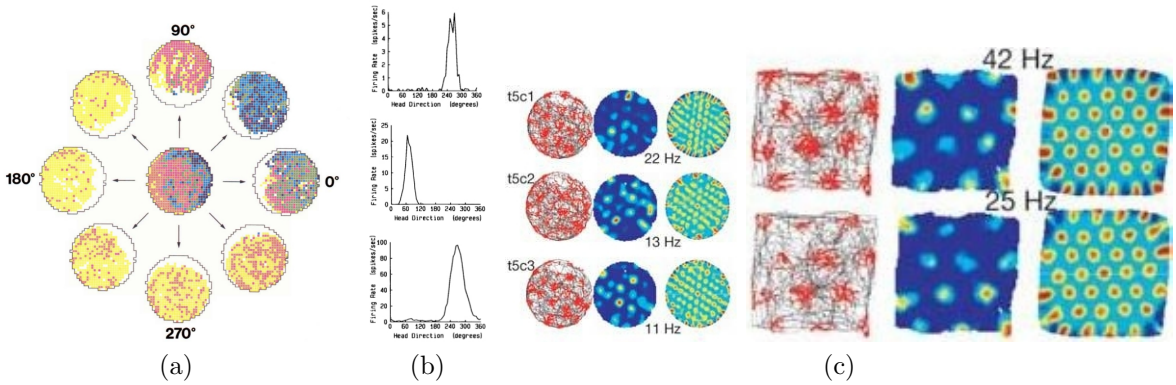

Figure 2.8: (a) Heat map of cell firings as a function of location and head direction. (b) Tuning curves for representative head direction cells. (c) Grid cell firing patters. (Taube et al., 1990; Hafting et al., 2005)

claim that place cell information is combined into a map-like cognitive structure.

For example, place cells have some properties that make them less-than-ideal units for a cognitive map. They are not logically ordered within the environment—nearby place cells do not necessarily have nearby place fields (O'Keefe and Conway, 1978). Place fields are not uniformly spaced throughout the environment as might be expected of an effective map; instead, place fields are highly clustered (Eichenbaum et al., 1989). Depending on the shape of the environment, they can be more likely to be near the border than at the environment's center, and they can be more likely to be near visual cues, such as posters on a curtain surrounding the environment (Hetherington and Shapiro, 1997). Holes in place field coverage due to clustering would amount to blind-spots in the map, which is not a particularly desirable property for a map to have.

Experimental evidence questions whether the local spatial information encoded by hippocampal cells are actually integrated into a map-like cognitive representation. A 1987 study by Muller and Kubie shows that most place cells lose or change their place fields when the environment grows (Figure 2.9). Spatial fields can be tied to cues rather than positions in the environment, meaning that moving the cue in a static environment changes the place fields (see Eichenbaum et al. 1999 or Section 2.5 on global remapping for further experimental evidence).

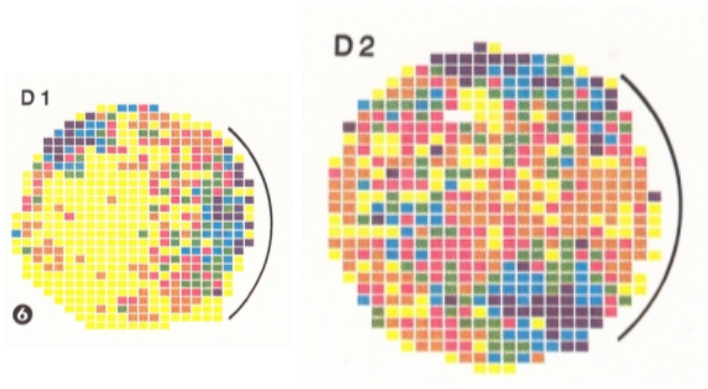

Figure 2.9: Changes in the place field of a single place cell due to environment scaling. Heat map represents firing rate. Purple squares are high rates, yellow are low. Ratio of images is not to scale.

2.4.2 More than Spatial

In contrast to the ample evidence suggesting that hippocampal cells in general, and place cells in particular, do not encode purely spatial information very well (Section 2.4.1), there is an increasing list of features that place cells do encode. Some cells change firing rates in response to novel objects or have different firing rates for different behaviors. One example are 'misplace' cells, which fire when an animal goes to a specific location and either finds a new object or does not find a familiar one (O'Keefe, 1976). Another factor is fear: stable CA1 place cells in a rat can change firing locations after the rat undergoes electric shock (Moita et al., 2004). Furthermore, a place cell's firing rate sometimes depends on the direction that the rat enters a field rather than just the spatial location (Figure 2.10). In 1999, Wood et al. found that more than half of the recorded hippocampal place cells identified in their experiment responded exclusively to non-spatial characteristics such as odor, expectation of reward, or proximity to a non-spatial target regardless of where the target was physically located. Going even further, Wood et al. found that under certain circumstances, a single place field can have a different place field in the exact same environment and performing the exact same task. In this experiment, a rat was trained to continuously alternate between branches on a modified T-maze. Wood et al. found that many rat place cells consistently fired in the main branch only when the rat was going to turn

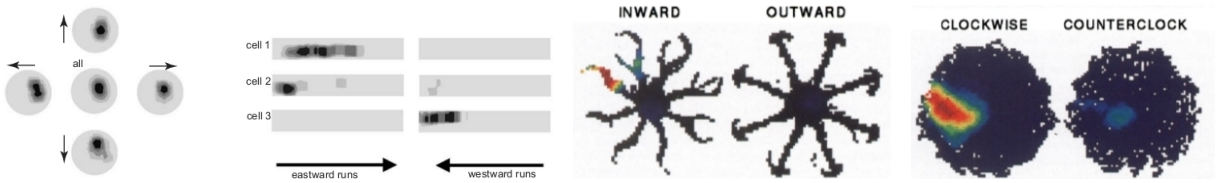

(a) (b) (c)

Figure 2.10: Place cells sometimes display directionality. (a) *Left* Place fields in open-field environments are nondirectional. *Right* Place fields on a directional track fire differently depending on the direction that the field is entered. (b) Place field locations change depending on whether a rat is running outwards or inwards in a radial maze. (c) Given certain task procedures, a rat can have different place fields in the clockwise and counterclockwise directions. (Andersen et al., 2007; Markus et al., 1995)

in one direction but not the other, despite the rat traveling in the same location, at the same speed, and performing the same task (Figure 2.11).

The lack of reliable spatial encoding and the clear preference for certain non-spatial encodings suggest that the term 'place cell' is something of a misnomer. Although there is universally accepted evidence that hippocampal place cell responses are linked to location, a more general theory is needed to explain the diverse range of place cell responses. One attempt to reconcile the memory and cognitive mapping explanations of the hippocampus is as follows:

"...true place cells are simply an example of the nodal codings that can identify past episodes that share a common event — in this case, a place experienced in the past. In this conception, other nodal codings, including those for a particular stimulus, similarly serve primarily as links to past episodes and not as parts of a spatial map. Nor are they used to navigate, except in the sense that memories for previous places and paths taken, as well as for the events that occurred in familiar locations, are useful for navigation and other forms of inferential memory expression." (Eichenbaum et al., 1999).

(a) (b) (c)

Figure 2.11: A task showing that a single place cell can have a different place field in the same environment while performing the same task. (a) Firing locations of a right-turn preferential cell. Left is the firing locations during the left turns (blue), and right is the firing location during right turns (red). (b) Firing locations of a left-turn preferential cell. Left is the firing locations during the left turns (blue), and right is the firing location during right turns (red). (b) The modified T-maze. (Wood et al., 2000)

2.5 Global Remapping

Places cells change in response to non-spatial stimuli (Section 2.4.2). This piece of evidence has been crucial in constructing a theory of hippocampal function that includes both memory and spatial phenomena - namely, that place cells in the hippocampus encode context rather than just location (Section 2.4). However, the process of a place cell changing its firing pattern, a process called 'remapping' (Bostock et al., 1991), is not yet well understood. Rather than trying to put forth a coherent theoretical framework for the remapping phenomenon, we will spend this chapter enumerating and describing relevant aspects of the phenomenon.

The first observation to note is that 'remapping' encompasses two related but distinct phenomena. 'Rate remapping' occurs when place field locations remain roughly unchanged, but the magnitude of the place cell's firing rate changes dramatically. 'Global remapping' occurs when both the place cell rates and the place field locations take on new statistically independent values (Leutgeb, 2005). The conditions under which each type of remapping occurs is different. In one study, experimenters induced each type of remapping in rats using slightly different experimental protocols. The variable-cue constant-place trials involved keeping a rat in the same room, but changing a salient visual cue such as changing the shape of the environment or the wall color. This induced CA1 place cell firing rates to diminish but essentially keep the same shape. In contrast, moving the rat from one room to another induced

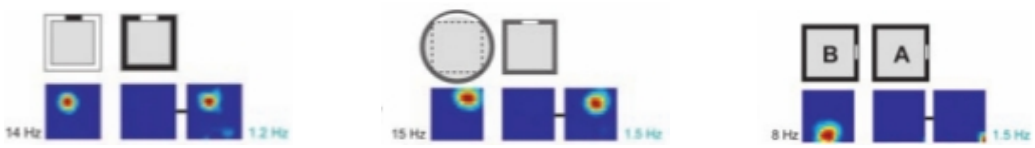

(a) (b) (c)

Figure 2.12: Examples of remapping. Heat maps of firing rates. Icon above firing rate maps indicate environment wall color or shape. Left column is original environment. Middle column is the rate map after changing the environment, with the color scheme the same as the first column. The right column is the same firing rate map as the second column but rescaled to the new peak firing rate. (a)(b) Rate remapping. (c) Global remapping.

a complete change in location and magnitude of the place fields, despite the rooms having the same color and shape (Figure 2.12).

Grid cells, like place cells, undergo changes in the spatial properties of their firing rates. In fact, grid cell remapping can be used to predict which type of remapping a place cell will undergo. Fyhn et al. (2007) showed that place cells globally remap when grid cells do, but only rate remap if the grid cells remained unchanged. Furthermore, the two processes happen roughly at the same time and on the same time scale, suggesting that perhaps there is a mechanistic link between the two processes. Grid cells are directly connected to the hippocampus (Witter, 2007), and computational models support the idea that grid cell remapping could indeed be the mechanism by which place cells remap (Fuhs and Touretzky, 2006; O'Keefe and Burgess, 2005).

Chapter 3

Experimental Techniques

In this chapter, we present background material regarding our experimental procedures. The two main tools we used to collect our data are tetrodes to record from the rat hippocampus (Section 3.1) and virtual reality to allow the rats to explore a large 2D environment (Section 3.2).

3.1 Recording from Cells

The recent advent of multi-electrode recordings (Wilson and McNaughton, 1993) has allowed scientists to simultaneously record from ensembles of neurons rather than just one at a time. This access to new data presents a new set of computational problems (Section 4.1) that, once overcome, allows new insight into how the brain is linked to behavior. One metaphor to describe this process is an orchestra: one can listen to any one single musician and learn about music, but you can't fully appreciate

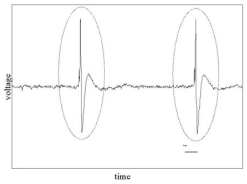

Figure 3.1: An example of a neuron action potential.

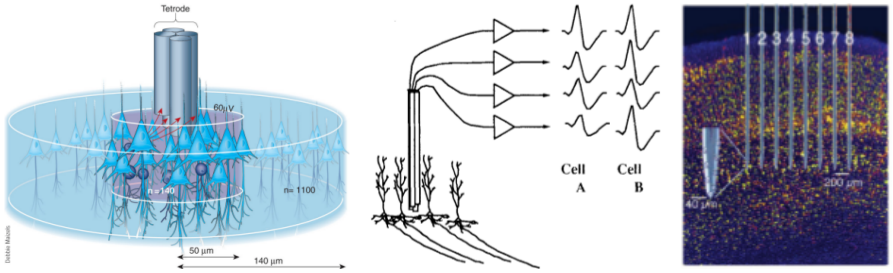

(a) (b) (c)

Figure 3.2: (a) A representation of an implanted electrode. (b) A schematic diagram of how the tetrode disambiguates cells. (c) Placement of an eight shank probe. (O'Keefe and Reece, 1993; Buzski, 2004)

an instrument's potential until you listen to every musician simultaneously (Buzski, 2004).

Brain cells, called neurons, communicate via electrical impulses called spikes or action potentials (Figure 3.2). The neuron's electrical potential fluctuates around some value until, as a result of the inputs to it from other neurons, the voltage rapidly rises to a peak far above the resting state. The neuron only briefly remains in this state of high electric potential, then quickly resets to its baseline value. The result of this spike is that an action potential travels down a projection from the neuron to other neurons, which then in turn interacts with that neuron's electric potential. The cascading effects of this process are how the brain encodes and reacts to stimulus.

One way to record this electrical activity is to put a conducting material, such as the tip of a wire, outside but near to the neuron (extracellular recording). If there are many neurons in the same area, then the conductor will record the electrical activity from all of them (Figure 3.2, left). Neurons of the same type generate the same shape action potential, so placing the conductor slightly closer to one neuron will measure a larger signal from it, distinguishing it from its neighbors (Figure 3.2, middle). While first implemented in the stereotrode in 1983 McNaughton et al., this principle was again implemented in a more modern tool called a tetrode (O'Keefe and Reece, 1993). In addition to discriminating the behavior of almost twice the number of cells as an electrode (Gray et al., 1995), tetrodes allow scientists to learn

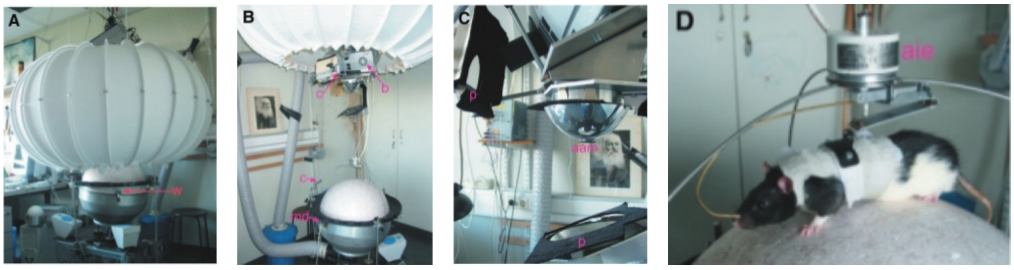

(a) (b) (c) (d)

Figure 3.3: The first rat virtual reality system. It overcame the difficulties of the rat's wide-angle optical system. (a) The system when the projection screen is in place surrounding the rat. (b) A view of the projector system when the screen is up. (c) The optical system in more detail. (d) A rat in its harness on the treadmill. (Hlscher et al., 2005)

about how populations of neurons behave, such as the sharp-wave ripple effect in the hippocampus that occurs when a rate is in slow wave sleep or immobile (Buzski et al., 1992).

3.2 Virtual Reality

Virtual reality (VR) systems are an invaluable scientific tool that can overcome many of the hurdles of conventional spatial experiments. VR has already been used in studies on how people navigate in space. Maguire et al. (1998) used VR to study how the human brain reacts to exploring a novel environment. They utilized the fact that humans 'exploring' VR are stationary, and as a result were able to take positron emission tomography (PET) measurements of the brain. Gillner and Mallot (1998) used a VR system to study how humans learn about spatial relationships in their environment. They were able to use the VR's controlled environment to restrict how much visual information a person received while exploring, and as a result they were able to show that humans are capable of learning about their surroundings from very little information.

Rats, too, have been studied using this technique. In 2005, Hlscher et al. developed the first rat-compatible VR system, overcoming the difficulties introduced by the rat's wide-angle vision system (Figure 3.3). They trained a control group of rats

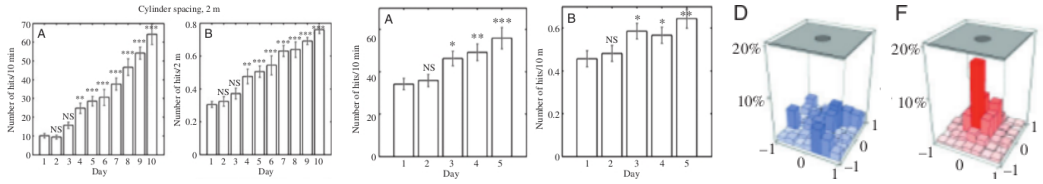

(a) (b) (c)

Figure 3.4: Time and accuracy results from rats trained in VR tasks. The improvement over time shows that rats can indeed learn to navigate VR environments. (a) Targets spaced 2m apart (easy). *Left.* Rats showing improvement in number of targets reached per unit of time. *Right.* Rats showing improvement in number of targets per distance covered. (b) Targets spaced 10m apart (hard). *Left.* Rats showing improvement in number of targets reached per unit of time. *Right.* Rats showing improvement in number of targets per distance covered. (c) Metric showing rats' performances improved. Graphs are histograms of fraction of time spent away from the nearest target. *Left.* Day 1. *Right.* After training. (Hlscher et al., 2005)

in a real 2m $\times$ 1.6m environment to retrieve a food reward below one of three types of cylinders. The cylinders were colored differently, and rewards only appeared below one type of cylinder. Within 4 days of trials, the rats had virtually stopped going to the non-reward cylinder. A second group of rats were tested on similar task in VR. The rats were placed into a harness on a rotatable sphere (treadmill) that spun when the rat walked to detect its motion (Figure 3.3).The rat was surrounded by a toroidal screen onto which the VR environment was projected. As the rat rotated its treadmill, motion sensors detect the movement and adjust the projected VR environment accordingly. Successful completion of a task triggered sugar water to flow to a valve near the rat's mouth.

In one virtual environment, the rats were tasked with seeking rewards below virtual cylinders. The environment was unbounded in the sense that running a certain distance in one direction brought the rat back to the starting point, and the cylinders were spaced 2m away from each other. The rats quickly learned to complete this task in a time and space efficient manner (Figure 3.4). A second virtual environment was identical to the first, except that the cylinders were spaced 10m apart instead of 2m. Although they did not perform as well on this difficult task, the rats showed improvement over the course of the trials (Figure 3.4). These VR tasks gathered data on rats moving in large environments; one radio-tracking study (Dowding and

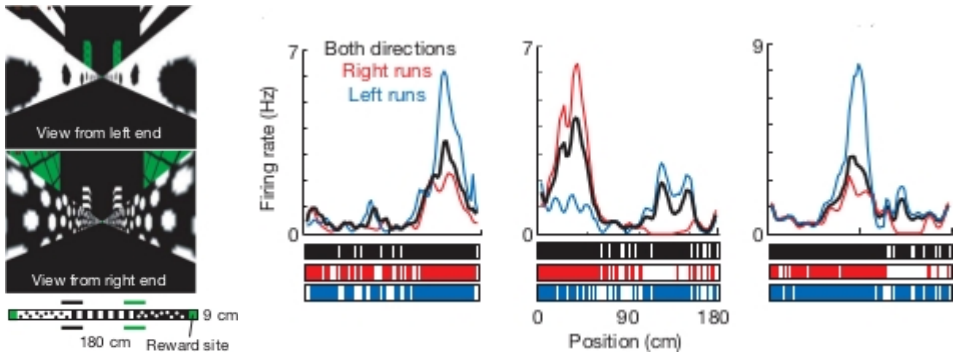

Figure 3.5: (a) The view from both ends of the virtual linear track. (b) Firing rate of three cells with respect to location on the linear track. These place cell readings show spatial specificity and directionality, which are two attributes of place cells in real life. This evidence suggests that place cells behave the same in VR as they do in real environments. (Harvey et al., 2009)

Murphy, 1994) indicated that rats naturally range over areas up to 1.85 $\times 10^5$ m^2, whereas traditional laboratory experiments limit rat movement to enclosures on the order of 1×1 m^2.

Another study (Harvey et al., 2009) utilized VR to take intracellular recordings of rats performing tasks on a linear track. The experimenters were able to identify CA1 place cells that responded to the virtual environment as if it were a real one. This is, the cells showed a firing bias towards a specific location on the track, and they showed directionality as is typical of place cells on a linear track (Figure 3.5). This result helped validate VR systems as a valid method of learning how place cells respond to natural environments.

Chapter 4

Computational Methods in Neuroscience

We present the reader with a brief overview of some relevant computational methods in neuroscience. Specifically, our discussion on spike sorting (Section 4.1) will help the reader understand how we arrive at our data before preprocessing (Section 7.1). Our section on context switching (Section 4.2) will help the reader understand how our method improves on previous methods.

4.1 Spike Sorting

It is one of the central tenets of modern neuroscience that the brain transmits information using electrical impulses called spikes. However, the brain is a complicated network of cells called neurons, and it can be very difficult to interpret electrical measurements because they reflect the activities of many neurons. Connections from one neuron extend to interact with other neurons, sending spikes along the projection that affect the electrical activity of other neurons. An electrical recording in the brain might reflect the spiking activity of one or more cells near the electrical probe in addition to the electrical outputs of other neurons that send projections into

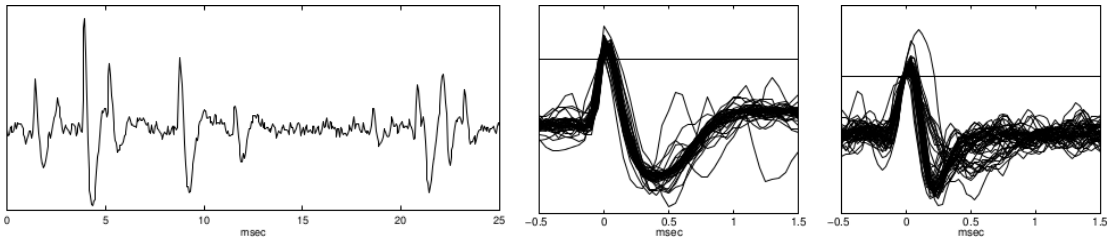

(a) (b)

Figure 4.1: (a) An extracellular waveform from a zebra finch forebrain showing action potentials from an unknown number of neurons. (b) *Left.* An oscilloscope trace of a well isolated neuron. A trace is shown every time the voltage went above the threshold. *Right.* An oscilloscope trace of a poorly isolated neuron. (Lewicki, 1998)

the probe's vicinity. Determining which part of an electrical recording represents the spiking activity of which cell is not a trivial task. This section presents an overview of a computational tool called spike sorting that helps to solve this problem (for a further motivation and a more detailed background description, see Section 3.1 on page 16).

4.1.1 Detecting Spikes

Before spiking activity can be labeled, it must first be detected. This process is complicated by the fact that there is background noise, spikes might change shape over time, and cell spikes might overlap. However, most spikes are recognizable by their high amplitudes — thus, one simple method of detecting spikes is to set a voltage threshold (Lewicki, 1998). The prediction is that voltage above the threshold indicates a spike, and below indicates no spike. The neuron of interest must be sufficiently isolated from its surrounding neighbors in order for the voltage reading to be a sufficient indicator of spiking (Figure 4.1). This process runs into the difficulty of overlapping activity from different neurons; the spike of one neuron coinciding with a dip in the background activity of other neurons might lead to the spike going undetected. More sophisticated techniques are necessary to overcome these difficulties.

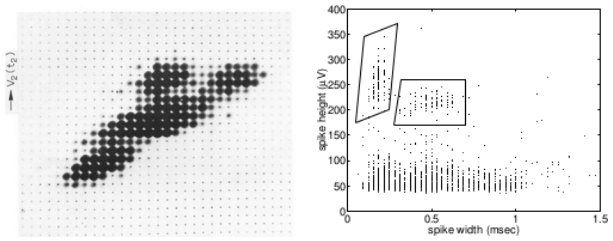

(a) (b)

Figure 4.2: (a) A histogram feature plot in a 1964 paper describing waveform feature extraction on a computer with 2000 bytes of memory. (b) A scatter plot of extracted 2D feature vectors. Potential cell clusters are circled. (Simon, 1964; Lewicki, 1998)

4.1.2 Labeling Spikes

Once spikes are identified, we need to accurately assess which spikes come from the same neuron. One method of identification is called feature analysis. This is the basic feature extraction technique in machine learning (Chapter 6) applied to spikes. Properties of the spike like minimum voltage, maximum voltage, or spike width are encoded into a feature vector. This method has a long history (Simon, 1964), and varying degrees of success have been achieved based on the data set and features extracted.

Once the spikes have been reduced to vectors in feature space, various methods of classification are possible. One such method is called 'cluster cutting' (Lewicki, 1998), and it involves a scientist manually drawing the boundaries for cell classification. A feature vector that falls in a particular region is classified as coming from one cell, whereas another cell might have another region in feature space (Figure 4.2). Other clustering methods from the machine learning literature are possible, and dimension reduction techniques such as Principal Component Analaysis (PCA) can be used in conjunction.

A second method of spike clustering falls into the category of filter-based methods. This class of sorting algorithms create a function called a filter that identifies each spike from other spikes and background noise (Roberts and Hartline, 1975). Although these methods achieve good results, they are more computationally intensive than

most feature extraction techniques and therefore are less suitable for classifying spikes in real-time (Gozani and Miller, 1994). One such filter construction method creates a linear filter, and it relies on four assumptions. First, we must assume that the spiking outputs of different cells add linearly in the output of the recording instrument. This is usually reasonable since electromagnetic waves in a conducting material generally add. Second, a single cell must have a spiking output that is constant in time. That is, the cell cannot have one waveform on its first spike and a radically different one on its next spike. Third, the background noise is random, but does not change properties over time, and is not correlated to the spiking activity. The fourth assumption is that cell spiking output waveforms are unique - they must be distinguishable from one another. Under these four assumptions, a single electrode's recording will be the following (Gozani and Miller, 1994):

$$r(t) = \sum_{i=1}^{m} \sum_{j=1}^{p_i} w^i(t - \tau_{ij}) + n(t) \tag{4.1}$$

In this equation, $r(t)$ is the electrical activity recorded on the electrode. i indexes a particular cell, and j indexes a particular spike. τ_{ij} is the time of the j^{th} spike from cell i, and $n(t)$ is the random noise. The function $w^i(t)$ is the shape of the spike of the i^{th} cell. Ultimately, $w^i(t)$, called the 'template', is the piece that we are trying to understand. By constructing a function for a single cell whose convolution with the electrode's recording is high when that cell fires and is low everywhere else, we can determine the spike times τ_{ij} with high accuracy (Figure 4.3). Solving an optimization problem that minimizes the filter's output to other cells subject to the constraint that its output on its own cell is sufficiently high will yield such a function (Gozani and Miller, 1994).

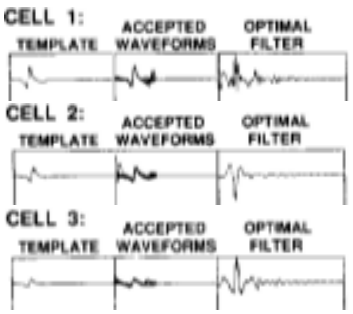

Figure 4.3: The set of templates and filters from three cells. *Left column.* The template derived for each cell. *Center column.* A linear superposition of all spikes from that cell. *Right column* The linear filter calculate for that cell. (Gozani and Miller, 1994)

4.2 Classifying Context Switches

Jezek et al. (2011) conducted an experiment to examine the phenomenon of global remapping (Section 2.5). To collect data, they trained rats in two different boxes with different external cues. After several days of training in two separate rooms, the cues in the rat's current room were suddenly switched to the cues of the second. This process effectively 'teleported' the rat from one room to another, inducing global remapping . The experimenters then sought to isolate the rat's hippocampal activity precisely at the moment when the place cells remapped. To do so, they attempted to use CA3 place cell activity to classify time periods into 'A' or 'B' contexts (for a general treatment of the classification problem, see Section 6 on page 31).

To compute the classifications, Jezek et al. used a dot product (DP) method to classify time periods according to which context a rat was in. They began by calculating 'baseline firing activities' for the cell populations during trials where the context was known (labeled data). To do so, they subdivided the environment into bins and calculated the mean firing rate for each bin and each context. The j^{th} cell in the i^{th} bin in context A was calculated to be the total number of spikes during the rat's time in bin i during context A divided by the total amount of time spent in bin i while in context A:

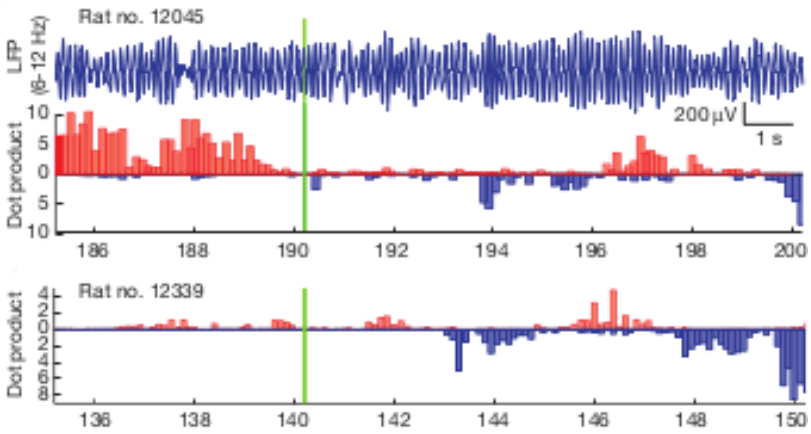

Figure 4.4: Results from the DP classifier showing context switching. Green line indicates when the 'teleportation' occurred. (Jezek et al., 2011)

$$r_i^A(j) = \frac{(\text{cell j spikes})_i^A}{\Delta t_i^A} \tag{4.2}$$

The collection of all such cells yields a vector of cell firing rates for each bin during each context. If we call this vector $\boldsymbol{r_i^A}$, then we have that the j^{th} component is $f_j^A(i)$ as calculated above. The same was done for context B.

Once these baseline firing rate vectors were calculated using labeled data, time periods were classified by the dot product of the current firing rate with the two baselines. Specifically, the authors split the trial into short epochs of about .25s and calculated the population firing rate vector $\boldsymbol{r}$ during each epoch. The classifier makes a decision based on the magnitude of the dot product between the population vector and each of the baseline vectors in the same spatial bin. If there are m cells in the recorded population and we let r^A and r^B be the baseline vectors for the current bin, then the decision rule for their classifier $C : (\mathbb{R}^+)^m \to \{A, B\}$ can be written as follows:

$$C(\boldsymbol{r}) = \begin{cases} A & : \boldsymbol{r} \cdot \boldsymbol{r^A} > \boldsymbol{r} \cdot \boldsymbol{r^B} \\ B & : \boldsymbol{r} \cdot \boldsymbol{r^A} < \boldsymbol{r} \cdot \boldsymbol{r^B} \end{cases}$$

The boundary situation when $\boldsymbol{r} \cdot \boldsymbol{r^A} = \boldsymbol{r} \cdot \boldsymbol{r^B}$ can be decided arbitrarily. The

results of their classification method show the time frame in which context switches occur (Figure 4.4).

Chapter 5

Experimental Setup

In this experiment, we explored global remapping in the hippocampus (Section 2.5, page 14) by examining neural data taken from rats performing tasks in virtual reality (VR). The system used was designed by Dmitriy Aronov (unpublished). Like similar systems, this VR system allows accurate neural recordings to be made during spatial tasks and allows experimenters to have complete control over the environment (for background on VR systems, see Section 3.2 on page 18). Unlike many other systems that require the rat to be head-fixed, this system allows rats to rotate a full 360° while in the machine, allowing them to explore a virtual 2D environment in an unconstrained manner. A fluid reward system rotates with the animal. In addition to the projection system covering 360° in the plane parallel to the ground, the system covered -30° to +45° in the elevation view. The resolution of the screen is greater than 1 cycle per degree, which is roughly the spatial frequency of the rat (Prusky et al., 2000). The cycle per degree measures an eye's ability to distinguish objects in terms of visual angle.

The rat is positioned on top of a spherical treadmill (similar to Figure 3.3, D on page 18) that rotates when the rat walks or runs. Software keeps track of treadmill's rotation, computes the image of the virtual environment from the rat's perspective,

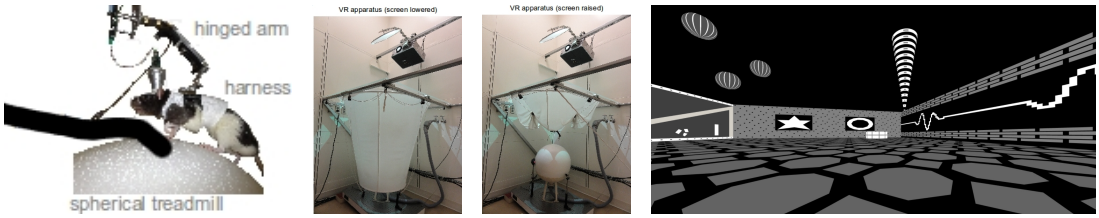

Figure 5.1: Images of our VR experimental setup. (a) A schematic diagram of the rotatable head fixture. (b) The VR system with the projector screen unrolled. (c) The VR system with the project screen rolled up. (d) A snapshot of the 2D virtual environment from the rat's vantage point. (Aronov and Tank, 2013)

warps the view to fit the screen's geometry, then projects the view via the projector. The rat walking forward on the treadmill, for example, would change the projected environment as if it was walking through the virtual space at the same velocity measured by the rotating treadmill. In this way, the rat could effectively interact with and explore a completely virtual 2D environment.

After construction, experiments validated that rats could be trained to move through a large enough portion of the environment. In the 'random foraging' task, a randomly selected sector of the environment was chosen so that the rat, upon entering the sector, would receive a drop of water. The sector was then randomly assigned to a different sector. The sector divisions and reward region were not visible to the rat. Environments were either a 1×1m square, a 2×2m square, a 1.4 m diameter circle, or a 2.8 m diameter circle. In a 2×2 m environment, the rat visited more than 90% of the environment within 20-30 minutes, confirming that the rat was capable of navigating in the virtual reality apparatus (Aronov and Tank, 2013).

In addition to the movement and vision components of the system, tetrodes were inserted into the rat to measure brain activity while it was interacting with the VR environment (for more information on tetrodes, see Section 3.1 on page 16). 8 or 16 tetrodes were placed in either CA1, CA3, or the MEC. These tetrodes recorded from the rat while it performed a clockwise or a counterclockwise 'target pursuit' task in a circular environment. In these tasks, the reward zone was marked by a

cylinder that was visible to the rat. As in the random foraging task, the rat received a water reward when it entered the vicinity of the cylinder. The cylinder was then moved some distance either clockwise or counterclockwise depending on the task. The cylinder was still visible to the rat, and a reward was only given if the rat approached the cylinder from the correct orientation — that is, if the rat moved too far in the clockwise direction during the counterclockwise task, the target would relocate so as to always be counterclockwise from the rat.

After the rats became comfortable with the two tasks, we began alternating tasks to induce global remapping. After some period of time giving the rat the clockwise task, for example, the marker would suddenly appear behind the rat and the software would enter into the counterclockwise task. The rat then recognized that the new task had begun and would reverse direction. At the same time, the changing task caused the rat to undergo a context shift, which would cause its place cells to remap. We sought to use the place cell recordings to accurately identify the moment(s) in time during which this remapping took place in order to better understand how the process occurs.

Chapter 6

Classification Overview

In this section, we will introduce and define some of the formal terminology used in the general classification problem. An application of this theory can be found in Section 4.2 on page 25 and in Chapter 7 on page 38.

The problem of classification involves assigning a label to each item in a set. Assigning quality ratings such as 'good' or 'bad' to movies is one instance of classification. 'Examples' are the data items used for learning or evaluation. In the instance we gave before, the movies themselves would be the examples. 'Features' are a set of attributes that are associated with an example, and they are most often represented as a vector. Some features one might choose for a movie are title, length, and the number of famous actors or actresses in the movie. 'Labels' are the values assigned to the examples. In our case they are the quality labels 'good' and 'bad'. Classification problems with only two labels are called 'binary classification' problems, and we will restrict our attention to problems in this category. The 'loss function' is used to measure the accuracy of a classifier. It takes a correct label and a predicted label as inputs, and outputs the difference or 'loss' between them. In binary classification problems, the lost function is most often the '0-1' loss function, which is 1 if the label is incorrect and 0 if it is correct (Mohri et al., 2012).

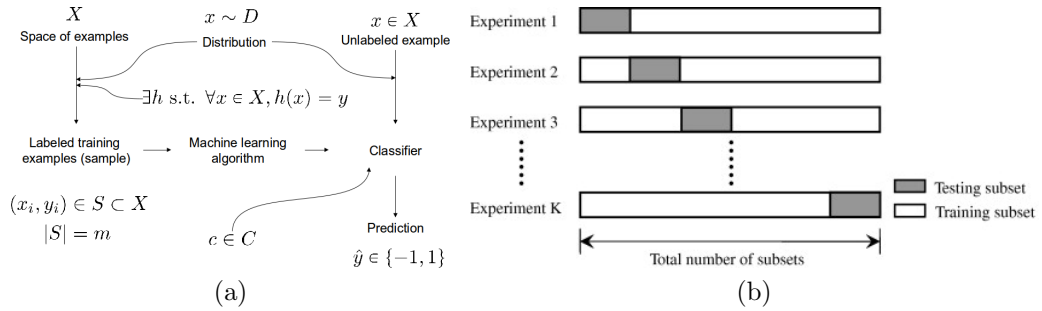

Figure 6.1: (a) A representation diagram of the supervised binary classification problem. Mathematical terminology is introduced in this diagram. (b) A pictorial representation of k-fold validation. This is the method used to estimate the generalization error of our algorithms.

The 'training sample' is the collection of examples and their correct labels that we will use to predict the correct labels on samples with unknown labels. We will use an algorithm that takes the training sample as input and produces what is called either a 'classifier', 'hypothesis' or a 'prediction rule', all of which are a function that takes examples as input and outputs a predicted label. Our 'validation sample' will be used to tune the parameters of the classifier. The 'test sample' are labeled examples used to evaluate the performance of the classifier. Test samples are not used producing the classifier and are used to estimate the classifier's error on the set of examples as a whole. Lastly, a 'hypothesis set' is a collection of possible classifiers (ie a set of functions that map examples to labels). One hypothesis space is the collection of hypotheses that label the movie 'The Matrix' as 'good'. Note that this is not just one classifier, but a collection of classifiers (Mohri et al., 2012).

In many situations, the data set is too small to set aside a validation sample, since doing so might make the training set too small to produce a good classifier. A technique called 'k-fold validation' can be used in this situation to combine the training and validation stages. The process begins by splitting the set of labeled examples into k subsamples, or folds. For each fold, the algorithm is trained on all but that fold, and the resulting classifier's accuracy is tested on the left-out fold. The parameters of the model are then chosen to minimize the 'cross-validation error', or the average of the classifier errors produced at each step. If the parameters of the

model are denoted by $\boldsymbol{\theta}$, then the value we wish to minimize is

$$\hat{R}_{CV}(\boldsymbol{\theta}) = \frac{1}{k}\sum_{i=1}^{k}\frac{1}{m_i}\sum_{j=1}^{m_i} L(h_i(x_{ij}), y_{ij}) \tag{6.1}$$

m_i is the size of the i^{th} fold, h_i is the classifier produced by leaving the i^{th} fold out of training, L is the loss function, and (x_{ij}, y_{ij}) is an example with its correct label.

Note that this method can also be used evaluate performance. If we fix the model parameters instead of varying them, we can evaluate the model using the cross-validation and the standard deviation across folds.

6.1 Types of Errors

Generalization is the way we measure accuracy of our classifier. It is the error that a classifier c makes on the entire space fo examples:

$$R(c) = \Pr_{x\sim D}[c(x) \neq y] \tag{6.2}$$

This problem is circular, in the sense that we must know how every example is actually classified in order to calculate this value. Thus, we instead use an estimate called the training error. This is the error that our classifier obtains on the training set. While it is usually calculated as the fraction of mistakes on the training error, you can view it as the generalization error over a distribution that only takes values on the training set:

$$\hat{R}(c) = \Pr_{x\sim U(S)}[c(x) \neq y] = \frac{1}{m}\sum_{i=1}^{m} \mathbb{1}_{c(x)\neq y} = \frac{1}{m}\sum \text{c's mistakes} \tag{6.3}$$

where $\mathbb{1}_{c(x)\neq y}$ is an indicator variable that is 1 if the classifier predicts incorrectly and 0 otherwise. $U(S)$ is the uniform distribution over the sample set, with a $\frac{1}{m}$ probability of picking any training example and a 0 probability of picking any other

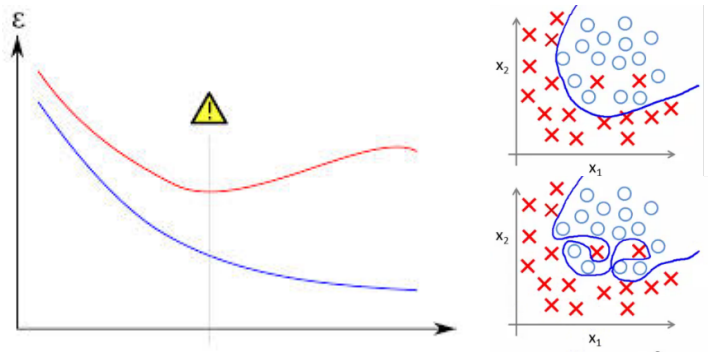

(a) (b)

Figure 6.2: (a) An example of overfitting. The x-axis represents model complexity, while the y-axis represents error. The hazard sign indicates the point at which a more complicated model might decrease training error, but will increase generalization error. (b) Two models, where one is intuitively 'more correct' than the other, which gets a lower training error score but obviously overfits.

example.

6.2 Overfitting

Overfitting is a problem in any machine learning context. Models with higher complexity usually can achieve a lower training error than simpler ones, but they don't always achieve a lower generalization error. At some point, more complex models achieve higher generalization errors (Figure 6.2). This intuition, often described in science as 'Occam's Razor', can be described mathematically. The expression, also called 'Occam's Razor', bounds the generalization error with the training error and model complexity. With probability $1 - \delta$, the following statement holds:

$$R(c) \leq \hat{R}(c) + \mathcal{R}(C) + \sqrt{\frac{\log \frac{1}{\delta}}{2m}} \tag{6.4}$$

$R(c)$ and $\hat{R}(c)$ are the generalization and training errors, respectively. $\mathcal{R}(C)$ is a measure of the complexity of the classifiers called the 'Rademacher complexity' (Mohri et al., 2012), and m is the number of training examples.

6.3 Exponential Family

The exponential family of probability distributions are commonly encountered in science. They include the most commonly seen ones such as the normal, Bernoulli, Poisson, binomial (with fixed number of trials), and multinomial (with fixed number of trials) distributions. Since this project explores two of these distributions in the context of neuroscience, we will make claims about the exponential family of distributions and apply the claims to the Poisson and Binomial distributions as special cases rather than derive the claims about each distribution separately.

Exponential family distributions in a single variable with one parameter (θ)can be written in the following general form:

$$p(x|\theta) = h(x)g(\theta)e^{\theta u(x)} \tag{6.5}$$

where the functions are chosen so that the resulting distribution is properly normalized.

Binary classification problems drawn from exponential families take a particularly simple form. If we make the notational switch into a binary classification problem where $\theta = \{a, b\}$, where the values correspond to the two labels, A, B, then we can minimize the generalization error to obtain an 'optimal classifier':

$$
\begin{aligned}
&Pr[x|A] \text{ is an exponential family distribution} \Rightarrow \\
&c_{opt}(x) = \begin{cases} A & : w_0 + w \cdot x^u > 0 \\ B & : w_0 + w \cdot x^u < 0 \end{cases} \\
&x^u = u(x) \\
&w_0 = \ln\left(\frac{Pr[A]}{Pr[B]}\right) + \ln\left(\frac{g(a)}{g(b)}\right) \\
&w = a - b
\end{aligned}
\tag{6.6}
$$

It is slightly artificial that this form looks like it is linear in x because the function u can be nonlinear. However, this term is linear for the Poisson and binomial distributions, so the resulting classifier is a hyperplane.

6.4 Naive Bayes Assumption

Multivariable classification problems with examples drawn from complex distributions can quickly become intractable. In order to make headway on these problems, it is often necessary to make simplifying assumptions. One commonly made assumption is called the 'Naive Bayes Assumption'. Although it is almost never true in practice, it has the virtues of being simple, easy to understand, and surprisingly successful.

The assumption is that components of the examples are independent conditioned

on the parameter. In our mathematical notation, this is written as:

$$x = \begin{pmatrix} x_1 \\ x_2 \\ ... \\ x_k \end{pmatrix}, \theta = \begin{pmatrix} \theta_1 \\ \theta_1 \\ ... \\ \theta_k \end{pmatrix} \tag{6.7}$$

$$Pr[x_i|\theta, x_j] = Pr[x_i|\theta_i], i \neq j$$

The intuition is that the parameter, which is now a , contains all of the information necessary to completely determine the distribution for each component. Said another way, knowing something about a different component does not add any new information.

Chapter 7

Analysis

The analysis of our data occurred in four steps. First, we processed our raw data (Section 7.1). Then, we took the resulting data and generating population vectors that could be used for classification (Section 7.2). We describe our method of calculating firing rates from population vectors (Section 7.3). Lastly, we describe our classification algorithm and how we implemented it (Section 7.4).

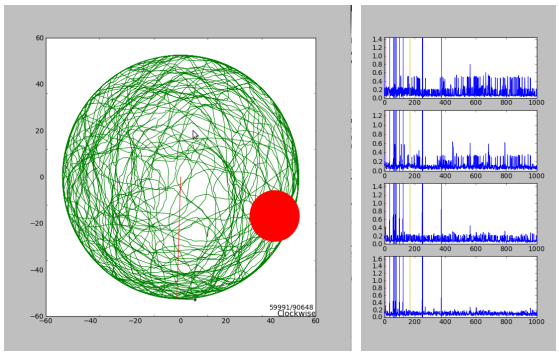

(a)

Figure 7.1: Custom-made software to visualize rat behavior in virtual reality along with cell spiking behavior. Black arrow indicates rat's position and velocity. Red circle is virtual marker the rat is chasing. Green lines indicates the rat's previous path.

1 = clockwise
-1 = counterclockwise

Clusters (cells)
1
2
3
...
46

Cluster	Position (in)	Task
1,2,3	(-7.9, 26.1)	1
	(-7.7, 26.6)	1
	(-7.3, 27.1)	1
1,3	(-6.9, 27.7)	1
	(-6.4, 28.3)	1
	(-6.0, 28.8)	-1
1,2,3	(-5.6, 29.4)	-1
	(-5.2, 29.9)	-1
1,3	(-4.8, 30.4)	-1
1,4,5,6	(-4.0, 31.5)	-1

(a) Example data.

Number of animals:	7
Number of sessions:	163
Average number of cells per session:	13.9
Max number of cells:	72
Average number of points per session:	98,000
Max number of points per session:	122,000

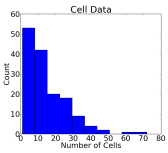

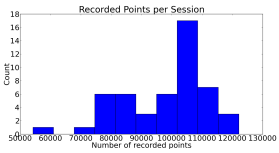

(b) Data statistics.

7.1 Data Preprocessing

We began by taking the signals recorded from the 16 tetrodes implanted in the rat's CA1 and CA3 (Chapter 5) and converting them to sequences of spike events using a linear filter (Section 4.1) called the Parks-McClellan optimal FIR filter (Parks and McCLellan, 1972). We considered events to be spike events if the response to a filter was three standard deviations away from the mean response. We then converted each spike event into a 4-dimensional feature vector. Each dimension of the feature vector was the difference between the maximum and minimum voltage on one electrode in the tetrode that detected the spike. Cells were identified by manually identifying clusters in feature space (cluster cutting; see Section 4.1 on page 21). For an example of the data in this form, see Table 7.1a. See Table 7.1b for descriptive statistics.

Each tetrode gave us a sequence of time points labeled with the identity of the cell that spiked, and potential spike events were discarded if the rat's instantaneous velocity was less than 2 cm/s or greater than 100 cm/s (detection aberration). Thus, we converted the analog waveforms to 16 sequences of vectors in $\{0, 1\}^c$, where components were 0 or 1.

7.2 Generating Population Vectors

We need to convert the sequence of cluster, spatial, and task information into a form that can be used by a machine learning classifier. The key problem with using the data as is is that one moment of data does not contain very much information about

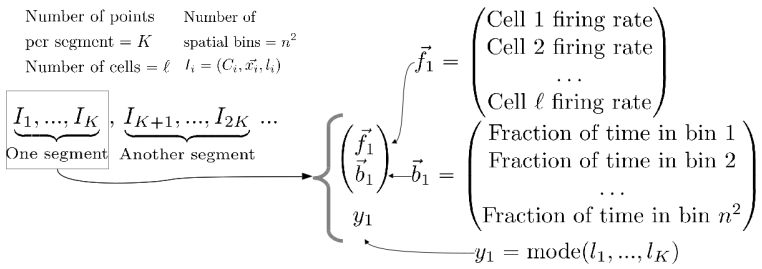

Figure 7.2: A graphical representation of turning spike trains into population vectors, which can then be used to train a classifier. If we use I_i to represent one moment of data, as in Table 7.1a, then we proceed by splitting the I_i's into groups of length K. Each group generates a single vector composed of firing rate information ($\boldsymbol{f_i}$), spatial information ($\boldsymbol{b_i}$), and label information (y_i).

the context. Place cells are not perfect indicators of position, and recording noise makes it seem like some cells spike when they are actually silent. Thus, we need an atomic unit that has more information. To achieve this, we group momentary data into groups and use them to generate 'population vectors' (Figure 7.2). These vectors contain all the relevant information about the firing rate of the cells during that period, as well as the spatial location and the identity of the task. The firing rate component consist of a single real number between 0 and 1 for each cell indicating the fraction of time that the cell was spiking. If the recordings have detected l different cells, then this component (indicated as $\boldsymbol{f_i}$ in Figure 7.2) is a vector in $[0, 1]^l$.

The next components of the population vector contains spatial information. Each component is the fraction of time that the rat spent in bin i during that group. Thus, if the environment is split into n^2 spatial bins, the spatial components ($\boldsymbol{b_i}$) are vectors in $[0, 1]^{n^2}$, where the components sum to 1.

Lastly, the correct label for the population vector is determined as the mode of the labels of the individual points. Since context switches happen infrequently, the individual labels often have the same identity.

7.3 Calculating Firing Rate Vectors

To estimate the firing rates of the recorded cells, we partitioned the environment into 2cm $\times$ 2cm bins and calculated the firing rate for each cell in each bin independently.

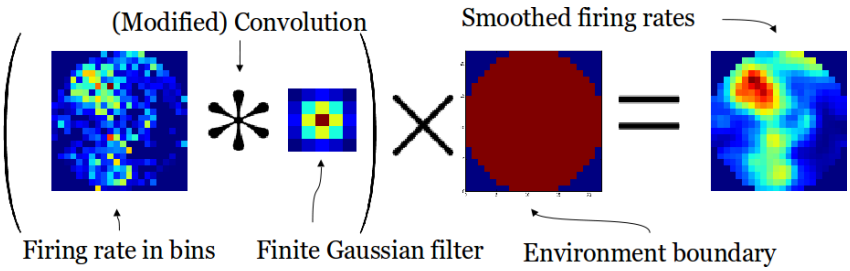

Figure 7.3: A graphical representation of the smoothing process. The left represents pre-smoothing. After a convolution with the discrete Gaussian kernel that is modified to take into account the circular nature of the environment, we multiply the result by a binary mask of the correct environment. The smoothed firing rates are on the right.

The firing rates were calculated in the same manner as Equation 4.2 (page 26). The spike count and time spent in each bin were calculated, then both were separately smoothed using a 10cm×10cm finite Gaussian filter as in Jezek et al. (2011):

$$\text{filter} = \begin{bmatrix} .0025 & .0125 & .0200 & .0125 & .0025 \\ .0125 & .0625 & .1000 & .0625 & .0125 \\ .0200 & .1000 & .1600 & .1000 & .0200 \\ .0125 & .0625 & .1000 & .0625 & .0125 \\ .0025 & .0125 & .0200 & .0125 & .0025 \end{bmatrix} \tag{7.1}$$

An example of firing rates before and after smoothing, as well as a graphical representation of the smoothing process, can be seen in Figure Figure 7.3.

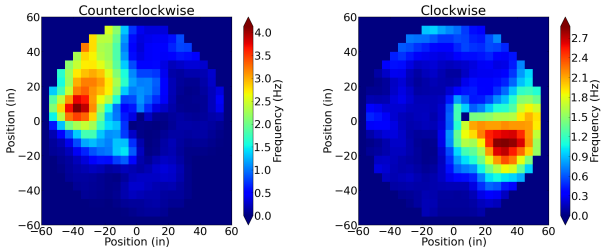

Figure 7.4: Representative spike rates for the same cell post smoothing in two different contexts.

7.4 Classification

We begin by noting that the dot product (DP) classifier (Section 4.2 on page 25) makes a decision rule by splitting feature space into two regions by a hyperplane through the origin. The general form for such a classifier is:

$$C(\boldsymbol{r}) = \begin{cases} A & : \boldsymbol{w} \cdot \ \boldsymbol{r} > 0 \\ B & : \boldsymbol{w} \cdot \ \boldsymbol{r} < 0 \end{cases}$$

In the case of the DP classifier, $\boldsymbol{w} = \boldsymbol{r^A} - \boldsymbol{r^B}$.

We next note that these two models are entirely data driven. That is, at no point do we use our knowledge of place cells or make any assumptions about the form of the data. While this keeps our algorithm general, we potentially lose accuracy by ignoring underlying patterns in the data. Making only the two assumptions that the cell firing rates are statistically independent (Naive Bayes) and that the cell firing rates come from a Poisson distribution (Zhang et al., 1998), we have that the classifier with the minimum generalization error is (for a proof, see Appendix A):

$$\begin{aligned} C(\boldsymbol{r}) &= \begin{cases} A: & w_0 + \boldsymbol{w} \cdot \boldsymbol{r} > 0 \\ B: & w_0 + \boldsymbol{w} \cdot \boldsymbol{r} < 0 \end{cases} \\ w_0 &= \frac{1}{\Delta t}\left[\ln\left(\frac{Pr[y=A]}{Pr[y=B]}\right) + |\boldsymbol{r^B}|_1 - |\boldsymbol{r^A}|_1\right] \\ w_i &= \ln\left(\frac{r_i^A}{r_i^B}\right) \qquad\qquad \text{for } i \neq 0 \end{aligned}$$

Here, $|\cdot|_1$ indicates the 1-norm. Δt is the time that each population vector spans, and $\boldsymbol{r_A}, \boldsymbol{r_B}$ are the true baseline firing rate vectors for the current bin during contexts A and B, respectively. Although we do not know the true firing rates, the purely data-driven estimate given in Section 4.2 is an unbiased estimator for the true value.

Chapter 8

Results

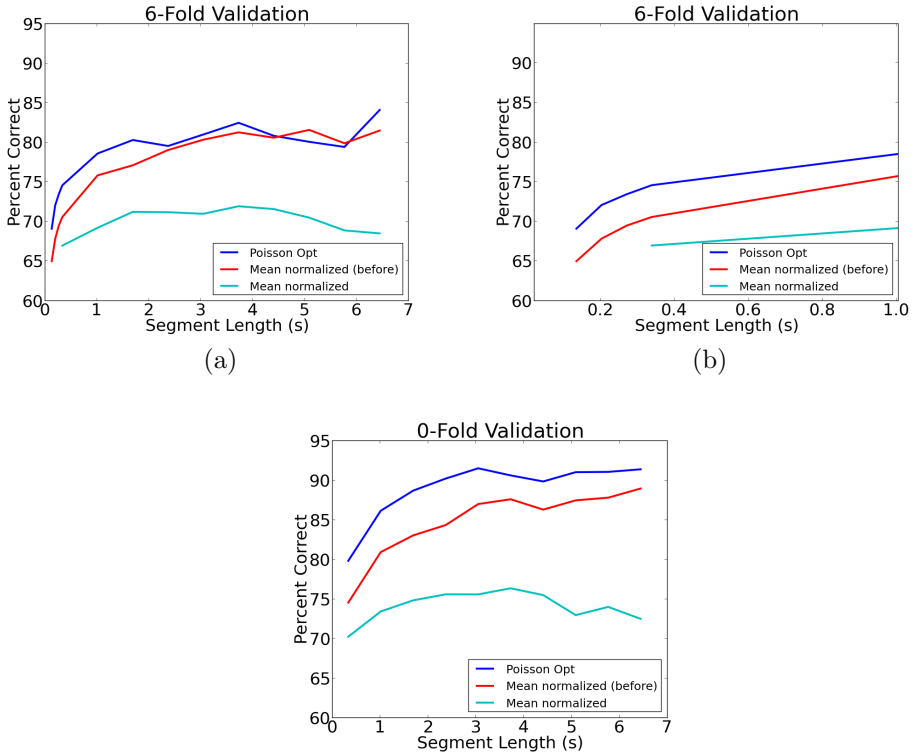

Figure 8.1: Simulation results for different classifiers. x-axis is the length of time used to generate the population vectors, and the y-axis is classification accuracy.

Our simulation results (Figure 8.1) show that the Poisson classifier is indeed more accurate than the previous classifier by Jezek et al. (2011). It shows a lower training

error (Figure 8.1c) and a lower generalization error according to 6-fold cross validation (Figure 8.1a). Furthermore, the neuroscientific goal of the classifier is to identify context switches in as temporally precise a manner as possible. The accuracy of the classifier is lower bounded by the amount of time that is combined into a single population vector. Thus, accuracy when the time segments are smallest is the most scientifically useful. The Poisson classifier's advantage is especially pronounced in this domain (Figure 8.1b).

Chapter 9

Discussion

We have shown through simulation and proof that, under certain well-used assumptions about place cell spiking, that our classifier will predict context switches more accurately than previous methods. Furthermore, this classifier is just as easy to compute, and works especially well when given less information. In addition, the model is based on biophysical assumptions rather than purely-data driven considerations. For example, other machine learning algorithms might be able to achieve higher prediction accuracies, but might not have easily interpretable parameters. Our model has parameters that are direct computations of factors about the place cells, whereas iterative learning methods can arrive at uninterpretable parameters.

Another very important advantage that our classifier has over previous work is that it adjusts to any number of firing rate maps regardless of whether they come from place cells or interneurons. The previous work, however, is much less robust to the high firing rates of interneurons, for example. The mean-normalized classifiers are modified versions of the DP classifier that allows them to handle interneuron data, but the classifier is useless on our full data set without this modification. Thus, it can be said that our classifier is more robust, in that it takes care of differences in mean firing rate in a natural way.

The assumptions used to calculate the optimal classifier are not universally valid. In particular, place cell activity can depend on a number of factors including the theta rhythm and direction into the field. Having a model with one parameter is convenient but inaccurate. Furthermore, the Naive Bayes assumption is violated both in the environment and in our method of calculating spike firing. In nature, exogenous variables influence and therefore probabilistically link spike firing. The hippocampus exhibits strong oscillatory behavior, which is exactly the kind of group behavior that violates the Naive Bayes assumption. The fact that our classifier performs well indicates that these assumptions might not be egregously violated, but more work needs to be done to determine which assumptions hold and which do not (Chapter 10).

Chapter 10

Future Work

This study can be extended in three directions. First, our classifier can be applied to the neural data to identify and explore the periods of time when context switching occurs. Second, we can extend our classifier to achieve even higher accuracy rates. Third, we can investigate the data to determine which of our assumptions are accurate and which do not hold.

Application

In the spirit of the motivation for this project, our classifier can be applied to the virtual reality data to explore whether context switching occurs in virtual reality the same as it does in laboratory settings. Such a study would prove interesting regardless of its outcome. Similarities between VR and lab context switching would more clearly define how well VR can be used a a testing tool, and differences in context switching have the possibility of exposing new hippocampal behavior.

Extension

More accurate models can easily be extended from this one. For example, a Bayesian treatment of the data would allow us to quantify the confidence of our classification. This could in itself be another method for determining context switching. More importantly, the Poisson model assigns nonzero probability to some events that have zero probability in our model. Given the way that we calculate population vectors, a cell can only spike a certain number of times during an interval. That is, if we are using K points to determine firing rate vectors, then a cell can spike at most K times. The Poisson distribution gives nonzero probabilities to the cell spiking $K+1$, $K+2$,... times. Thus, perhaps a binomial distribution on K trials would better fit the data. Although this is not the usual assumption, it does make sense given that the binomial distribution converges to the Poisson distribution under certain conditions.

Investigation

In pursuit of an even better classifier, it makes sense to investigate the validity of the assumptions necessary to calculating this classifier. For example, plotting a histogram of the number of spikes per firing rate vector in a given context in a given bin could validate or invalidate the assumption that firing is Poisson. Also, the Naive Bayes assumption could be statistically validated.

Appendix A

Deriving the Optimal Classifier

Each spatial bin can be thought of as its own classification problem. Thus, we restrict our attention to a single spatial bin. We formalize the problem as follows:

$$\mathbb{X} = (\mathbb{Z}_0^+)^M$$

$$\mathbb{C} = \text{Probabilistically assigns a label A or B}$$

where $\mathbb{X}$ is the space of examples, and $\mathbb{C}$ is the space of concepts that map examples to A or B. M is the number of cells, and feature vectors will be denoted $\boldsymbol{n} \in \mathbb{X}$, is a vector whose i^{th} component is the number of spikes for cell i. Note that for our problem, the examples vectors in $\mathbb{X}$ are vectors of the **number** of spikes in a given time period rather than the **rate**. If each spike vector was calculated in the same length time window, then the two vectors are related by the simple equation $\boldsymbol{r}\Delta t = \boldsymbol{n}$.

Then for any hypothesis $C \in \mathbb{C}$, we have that the generalized error is:

$$\begin{aligned} err(C) &= \left(\sum_{\boldsymbol{n}, C(\boldsymbol{n})=A} Pr[\boldsymbol{n}, y = B] \right) + \left(\sum_{\boldsymbol{n}, C(\boldsymbol{n})=B} Pr[\boldsymbol{n}, y = A] \right) \\ &= \left(\sum_{\boldsymbol{n}, C(\boldsymbol{n})=A} Pr[y = B] Pr[\boldsymbol{n}|y = B] \right) + \left(\sum_{\boldsymbol{n}, C(\boldsymbol{n})=B} Pr[y = A] Pr[\boldsymbol{n}|y = A] \right) \end{aligned}$$

Note that a deterministic hypothesis will label every example. Thus, every element will show up in either the left sum or the right sum. If we wish to minimize the overall error, we want to label the example with whichever label will minimize the contribution to the generalization error. This condition can be expressed as:

$$C_{opt}(\boldsymbol{n}) = \begin{cases} A: & Pr[y=B]Pr[\boldsymbol{n}|y=B] < Pr[y=A]Pr[\boldsymbol{n}|y=A] \\ B: & Pr[y=B]Pr[\boldsymbol{n}|y=B] > Pr[y=A]Pr[\boldsymbol{n}|y=A] \end{cases} \tag{A.1}$$

Now let us make the following assumptions about the set of examples and the concept class:

1. Each feature is independent of each other conditional on the label (Naive Bayes)
2. The probability of of seeing a particular value in the example vector is in the exponential class of families, with parameter dependent on the label.
3. The model takes a single parameter

The exponential family of distributions is an important class of distribution functions that encompasses many of the ones used in neuroscience such as the Poisson, Bernoulli, exponential, and multinomial (with a fixed number of trials) distributions. We will derive the optimal classifier under these general assumptions, then specify which exponential distribution we will apply after.

Exponential distributions take the following form (Bishop, 2006):

$$p(n|\theta) = h(n)g(\theta)e^{\theta u(n)} \tag{A.2}$$

where θ is the parameter of the model, and $h(n)$,$g(\theta)$, and $u(n)$ are functions that determine the distribution within the exponential family. Note that in this particular equation, we are assuming that n is a scalar.

The third assumption above says that our only parameter θ will be the firing rate of the cell. Although this assumption makes the problem easier to work with, the place cell behavior has been shown to depend on other factors such as the phase of the theta rhythm (O'Keefe and Reece, 1993).

Let a_i be the parameter for the i^{th} component of the vector if it is labeled with A, and b_i be the corresponding parameter if the label is B.

Together, our three assumptions imply

$$Pr[\boldsymbol{n}|A] = \prod_{i=1}^{M} h(n_i)g(a_i)e^{a_i u(n_i)}$$
$$Pr[\boldsymbol{n}|B] = \prod_{i=1}^{M} h(n_i)g(b_i)e^{b_i u(n_i)}$$

Applying this expression to Equation A.1, we get the following decision rule:

$$C_{opt}(\boldsymbol{n}) = \begin{cases} A: & w_0 + \boldsymbol{w} \cdot \boldsymbol{n^u} > 0 \\ B: & w_0 + \boldsymbol{w} \cdot \boldsymbol{n^u} < 0 \end{cases} \tag{A.3}$$

$$(\boldsymbol{n^u})_i = u(n_i)$$
$$w_0 = \ln\left(\frac{Pr[A]}{Pr[B]}\right) + \sum_{i=1}^{M} \ln\left(\frac{g(a_i)}{g(b_i)}\right)$$
$$w_i = a_i - b_i \qquad\qquad 1 \le i \le M$$

Note that this expression for the optimum deterministic hypothesis is a hyperplane in $\boldsymbol{n^u}$.

If we make the assumption that place cells spikes come from a Poisson process (Zhang et al., 1998) and switch from dealing with vectors of spikes to vectors of firing

rates, then this expression simplifies to:

$$C_{opt}(\boldsymbol{r}) = \begin{cases} A: & w_0 + \boldsymbol{w} \cdot \boldsymbol{r} > 0 \\ B: & w_0 + \boldsymbol{w} \cdot \boldsymbol{r} < 0 \end{cases} \tag{A.4}$$

$$w_0 = \frac{1}{\Delta t}\left[\ln\left(\frac{Pr[A]}{Pr[B]}\right) + |\boldsymbol{r^B}|_1 - |\boldsymbol{r^A}|_1\right]$$

$$w_i = \ln\left(\frac{r_i^A}{r_i^B}\right) \qquad 1 \le i \le M$$

In this expression, $\boldsymbol{r}$ is a vector of firing rates as measured from a time window of length Δt, and r_i^A, r_i^B is the true firing rate for the i^{th} cell in context A and B, respectively. $\boldsymbol{r^A}$ and $\boldsymbol{r^B}$ are vectors of the true firing rates. Note that the optimum deterministic hypothesis takes the form of a hyperplane with nonzero bias. Assuming an uninformative prior (uniform prior) over A and B simplifies the expression further.

Alternatively, we can tailor an algorithm more specific to our problem. We determine firing rates by taking a sequence of k consecutive points and counting the rate of spiking in that time window. Furthermore, each point can be labeled with at most one spike. Thus, we have a limit to the number of spikes that can occur in one sequence. That is, in our method of generating spike vectors, $Pr[n_i > k] = 0$, where n_i is again the number of spikes counted from cell i during our window. If we include the number of no-spikes that occur as an element in our vector $\boldsymbol{n}$, then we have a multinomial distribution on our spike counts. If we again let M be the number of detected cells, then we have a multinomial distribution on k trials with M+1 outcomes per trial. For $1 \le i \le M$, the i^{th} event means that the i^{th} cell firing at that moment. We let the $(M+1)^{th}$ event indicate that no cell fired. Using this distribution and

again converting to firing rates, we have the following optimal classifier:

$$
\begin{aligned}
C_{opt}(\boldsymbol{r}) &= \begin{cases} A: & w_0 + \boldsymbol{w} \cdot \boldsymbol{r} > 0 \\ B: & w_0 + \boldsymbol{w} \cdot \boldsymbol{r} < 0 \end{cases} \\
w_0 &= \frac{1}{\Delta t} \ln \left(\frac{Pr[y = F]}{Pr[y = G]} \right) \\
w_i &= \ln \left(\frac{r_i^A}{r_i^B} \right) \qquad\qquad 1 \leq i \leq M + 1
\end{aligned}
\tag{A.5}
$$

The change from a Poisson to a multinomial distribution alters the bias and adds 'silence' as a dimension in the feature vector.

Bibliography

Andersen, P., Morris, R., Amaral, D., Bliss, T., and O'Keefe, J., editors (2007). *The Hippocampus Book*. Oxford University Press.

Aronov, D. and Tank, D. W. (2013). Engagement of the circuits underlying 2d spatial memory in a virtual reality system designed for rats. Experiment Notes.

Bishop, C. M. (2006). *Pattern Recognition and Machine Learning*. Springer.

Bostock, E., Muller, R. U., and Kubie, J. L. (1991). Experience-dependent modifications of hippocampal place cell firing. *HIPPOCAMPUS,*, 1:193–206.

Buzski, G. (2004). Large-scale recording of neuronal ensembles. *Nature neuroscience*, 7:446–451.

Buzski, G., Horvth, Z., Urioste, R., Hetke, J., and Wise, K. (1992). High-frequency network oscillation in the hippocampus. *Science*, 256:1025–1027.

Cohen, N. J. and Squire, L. R. (1980). Preserved learning and retention of pattern-analyzing skill in amnesia: Dissociation of know how and knowing that. *Science, New Series*, 210:207–210.

Corkin, S. (2002). Whats new with the amnesic patient h.m.? *Nature Reviews Neuroscience*, 3:153160.

Douglas, R. J. (1967). The hippocampus and behavior. *Psychological Bulletin*, 67:416–442.

Dowding, J. E. and Murphy, E. C. (1994). Ecology of ship rats (rattus rattus) in a kauri (agathis australis) forest in northland, new zealand. *New Zealand Journal of Ecology*, 18:19–28.

Eichenbaum, H., Dudchenko, P., Wood, E., Shapiro, M., and Tanila, H. (1999). The hippocampus, memory, and place cells: Is it spatial memory or a memory space? *Neuron*, 23:209–226.

Eichenbaum, H., Wiener, S. I., Shapiro, M. L., and Cohen, N. J. (1989). The organization of spatial coding in the hippocampus: A study of neural ensemble activity. *The Journal of Neuroscience*, 9:2764–2775.

Fenton, A. A., Kao, H.-Y., Neyotin, S. A., Olypher, A., Vayntrub, Y., Lytton, W. W., and Ludvig, N. (2008). Unmasking the ca1 ensemble place code by exposures to small and large environments: More place cells and multiple, irregularly arranged, and expanded place fields in the larger space. *The Journal of Neuroscience*, 28:11250–11262.

Francesca Sargolini, e. a. (2006). Conjunctive representation of position, direction, and velocity in entorhinal cortex. *Science*, 312:758.

Fuhs, M. C. and Touretzky, D. S. (2006). A spin glass model of path integration in rat medial entorhinal cortex. *The Journal of Neuroscience*, 26:4266–4276.

Fyhn, M., Hafting1, T., Treves, A., Moser, M.-B., and Moser, E. I. (2007). Hippocampal remapping and grid realignment in entorhinal cortex. *Nature*, 446:190–194.

Gillner, S. and Mallot, H. A. (1998). Navigation and acquisition of spatial knowledge in a virtual maze. *Journal of Cognitive Neuroscience*, 10:445–463.

Gozani, S. N. and Miller, J. P. (1994). Optimal discrimination and classification of neuronal action potential waveforms from multiunit, multichannel recordings

using software-based linear filters. *IEEE Transactions on Biomedical Engineering*, 41:358–372.

Gray, C. M., Maldonado, P. E., Wilson, M., and McNaughton, B. (1995). Tetrodes markedly improve the reliability and yield of multiple single-unit isolation from multiunit recordings in cat striate cortex. *J. Neurosci. Meth*, 63:4354.

Hafting, T., Fyhn, M., Molden, S., Moser, M.-B., and Moser, E. I. (2005). Microstructure of a spatial map in the entorhinal cortex. *Nature*, 436:801–806.

Harvey, C. D., Collman, F., Dombeck, D. A., and Tank, D. W. (2009). Intracellular dynamics of hippocampal place cells during virtual navigation. *Nature*, 461:941–946.

Hetherington, P. A. and Shapiro, M. L. (1997). Hippocampal place fields are altered by the removal of single visual cues in a distance-dependent manner. *Behavioral Neuroscience*, 111:20–34.

Horel, J. A. (1978). The neuroanatomy of amnesia: A critique of the hippocampal memory hypothesis. *Brain*, 101:403–445.

Hlscher, C., Schnee, A., Dahmen, H., Setia, L., and Mallot, H. A. (2005). Rats are able to navigate in virtual environments. *The Journal of Experimental Biology*, 208:561–569.

Jezek, K., Henriksen, E. J., Treves, A., Moser, E. I., and Moser1, M.-B. (2011). Theta-paced flickering between place-cell maps in the hippocampus. *Nature*, 478:246–249.

Leutgeb, e. a. (2005). Independent codes for spatial and episodic memory in hippocampal neuronal ensembles. *Science*, 309:619–623.

Lewicki, M. S. (1998). A review of methods for spike sorting: the detection and

classification of neural action potentials. *Network: Comput. Neural Syst.*, 9:R54–R77.

Maguire, E. A., Frith, C. D., Burgess, N., Donnett, J. G., and OKeefe, J. (1998). Knowing where things are: Parahippocampal involvement in encoding object locations in virtual large-scale space. *Journal of Cognitive Neuroscience*, 10:61–76.

Markus, E. J., Qin, Y.-L., Leonard, B., Skaggs, W. E., McNaughton, B. L., and Barnes, C. A. (1995). Interactions between location and task affect the spatial and directional firing of hippocampal neurons. *The Journal of Neuroscience*, 15:7079–7094.

McNaughton, B. L., O'Keefe, J., and Barnes, C. A. (1983). The stereotrode: A new technique for simultaneous isolation of several single units in the central nervous system from multiple unit records. *Journal of Neuroscience Methods*, 8:391–397.

Mishkin, M. (1978). Memory in monkeys severely impaired by combined by not by seperate removal of amygdala and hippocampus. *Nature*, 273.

Mohri, M., Rostamizadeh, A., and Talwalkar, A. (2012). *Foundations of Machine Learning*. The MIT Press.

Moita, M. A. P., Rosis, S., Zhou, Y., LeDoux, J. E., and Blair, H. T. (2004). Putting fear in its place: Remapping of hippocampal place cells during fear conditioning. *The Journal of Neuroscience*, 24:7015–7023.

Moser, E. I., Kropff, E., and Moser, M.-B. (2008). Place cells, grid cells, and the brain's spatial representation system. *Annu. Rev. Neurosci.*, 31:69–89.

Muller, R. U. and Kubie, J. L. (1987). The effects of changes in the environment hippocampal complex-spike cells. *The Journal of Neuroscience*, 7:1951–1968.

O'Keefe, J. (1976). Place units in the hippocampus of the freely moving rat. *Experimental Neurology*, 51:78–109.

O'Keefe, J. and Burgess, N. (2005). Dual phase and rate coding in hippocampal place cells: theoretical significance and relationship to entorhinal grid cells. *Hippocampus*, 15:853–866.

O'Keefe, J. and Conway, D. H. (1978). Hippocampal place units in the freely moving rat: Why they fire where they fire. *Exp. Brain Res.*, 31:573–590.

O'Keefe, J. and Nadel, L. (1978). *The Hippocampus as a Cognitive Map*. Oxford University Press.

O'Keefe, J. and Reece, M. L. (1993). Phase relationship between hippocampal place units and the eeg theta rhythm. *Hippocampus*, 3:317–330.

Parks, T. W. and McCLellan, J. H. (1972). A program for the design of linear phase finite impulse response digital filters. *IEEE Transactions on Audio and Electroacoustics*, 20:195–199.

Prusky, G. T., West, P. W., and Douglas, R. M. (2000). Behavioral assessment of visual acuity in mice and rats. *Vision Research*, 4:2201–2209.

Ranck, J. B. (1984). Head-directioncells in the deep cell layers of the dorsal presubiculum in freely moving rats. *Soc. Neurosci.*, 10:599.

Roberts, W. M. and Hartline, D. K. (1975). Separation of multi-unit nerve impulse trains by a multichannel linear filter algorithm. *Brain Research*, 94:141–149.

Scoville, W. B. and Milner, B. (1957). Loss of recent memory after bilateral hippocampal. *J. Neurol. Neurosurg. Psychiat.,*, 20:11.

Simon, W. (1964). The real-time sorting of neuro-electric action potentials in multiple unit studies. *Electroencephalography and Clinical Neurophysiology*, 18:192–195.

Squire, L. R. (1987). *Memory and brain*. Oxford University Press.

Taube, J. S., Muller, R. U., and James B. Ranck, J. (1990). Head-direction cells recorded from the postsubiculum in freely moving rats. i. description and quantitative analysis. *The Journal of Neuroscience*, 10(2):420–435.

Tolman, E. (1948). Cognitive maps in rats and men. *Psychological Review*, 55:189208.

Tulving, E. (1972). *Organization of Memory*. New York: Academic Press.

Wilson, M. A. and McNaughton, B. L. (1993). Dynamics of the hippocampal ensemble code for space. *Science*, 261:1055–1058.

Witter, M. P. (2007). The perforant path: projections from the entorhinal cortex to the dentate gyrus. *Progress in Brain Research*, 163:43–61.

Wood, E. R., Dudchenko, P. A., and Eichenbaum, H. (1999). The global record of memory in hippocampal neuronal activity. *Nature*, 397:613–616.

Wood, E. R., Dudchenko, P. A., Robitsek, R. J., and Eichenbaum, H. (2000). Hippocampal neurons encode information about different types of memory episodes occurring in the same location. *Neuron*, 27:623–633.

Zhang, K., Ginzburg, I., McNaughton, B. L., and Sejnowski, T. J. (1998). Interpreting neuronal population activity by reconstruction: Unified framework with application to hippocampal place cells. *Journal of Neurophysiology*, 79:1017–1044.

Zola-Morgan, S., Squire, L. R., and Amaral, D. G. (1986). Human amnesia and the medial temporal region: Enduring memory impairment following a bilateral lesion limited to field ca1 of the hippocampus. *The Journal of Neuroscience*, 6:2950–2967.